InP/$Ga_{0.47}In_{0.53}As$ Monolithic, Two-Junction, Three-Terminal Tandem Solar Cells

M.W. Wanlass, T.A. Gessert, G.S. Horner, K.A Emery and T.J. Coutts
Solar Energy Research Institute
Golden, CO

Summary

The work presented in this paper has focussed on increasing the efficiency of InP-based solar cells through the development of a novel, high-performance InP/$Ga_{0.47}In_{0.53}As$ two-junction, three-terminal monolithic tandem cell. Such a tandem is particularly suited to space applications where a radiation-hard top cell (i.e., InP) is required. Furthermore, the InP/$Ga_{0.47}In_{0.53}As$ materials system is lattice matched and offers a top cell/bottom cell bandgap differential (0.60 eV at 300K) suitable for high tandem cell efficiencies under AM0 illumination. A three-terminal configuration has been chosen since it allows for independent power collection from each subcell in the monolithic stack, thus minimizing the adverse impact of radiation damage on the overall tandem efficiency. Realistic computer modeling calculations predict an efficiency boost of 7-11% from the $Ga_{0.47}In_{0.53}As$ bottom cell under AM0 illumination (25°C) for concentration ratios in the 1-1000 range. Thus, practical AM0 efficiencies of 25-32% appear possible with the InP/$Ga_{0.47}In_{0.53}As$ tandem cell.

Prototype n/p/n InP/$Ga_{0.47}In_{0.53}As$ monolithic tandem cells have been fabricated and tested successfully. Using an aperture to define the illuminated area, efficiency measurements performed on a non-optimized device under standard global illumination conditions (25°C) with no antireflection coating (ARC) give 12.2% for the InP top cell and 3.2% for the $Ga_{0.47}In_{0.53}As$ bottom cell, yielding an overall tandem efficiency of 15.4%. With an ARC, the tandem efficiency could reach ~22% global and ~20% AM0. Additional details regarding the performance of individual InP and $Ga_{0.47}In_{0.53}As$ component cells, fabrication and operation of complete tandem cells and methods for improving the tandem cell performance, are also discussed.

Introduction

Current strategies for increasing the power-to-mass ratio and end-of-life efficiency of space cells include the development of tandem cells, both monolithic and mechanically stacked (e.g., GaAs/Ge [ref. 1] and GaAs/$CuInSe_2$ [ref. 2], respectively), concentrator cells [ref. 3] and radiation-hard InP cells [ref. 4]. The work presented in this report is based on an approach which merges the above strategies into a single monolithic, three-terminal tandem device by combining an InP top cell with a lattice

matched, infrared-sensitive $Ga_{0.47}In_{0.53}As$ (hereafter GaInAs) bottom cell. Monolithic, two-junction, three-terminal tandem cells have been fabricated previously in the $Al_xGa_{1-x}As/GaAs$ [ref. 5] and $GaAs_xP_{1-x}/GaAs_ySb_{1-y}$ [ref. 6] materials systems. However, to our knowledge the present work constitutes the first report of monolithic tandems demonstrated in the lattice matched, InP-based $InP/Ga_xIn_{1-x}/As_yP_{1-y}$ materials system. In the remaining sections, the techniques used and progress made in the early development of this new tandem space cell are reviewed.

Device Concept

A schematic illustration of the InP/GaInAs three-terminal tandem cell structure is given in figure 1. In its simplest form, the device consists of four lattice matched epitaxial layers grown on a single-crystal InP substrate. The n^+/p InP top cell and p^+/n GaInAs bottom cell junctions are of opposite polarity in order to provide a common intermediate p-type region for placement of the middle contact, resulting in a transistor-like n/p/n overall doping configuration. In practical tandems, the middle contact is placed below the photoactive region of the InP top cell so as to avoid enhanced carrier recombination (i.e., the p-InP base layer is grown thicker than that necessary to provide complete optical absorption - this is described in more detail in following sections). Top and back contacts are placed on the front surface of the InP cell emitter and the back surface of the n^+-InP substrate, respectively. The three-terminal design offers special advantages with respect to both characterization of the component subcells and operation in space. Quantum efficiency and current-voltage measurements can be made on each subcell individually and independently due to the common middle terminal. Furthermore, through proper design of the middle contact (i.e., by minimizing the associated series resistance) the subcells can operate as if independently connected, thus minimizing the deleterious impact of radiation damage on the combined tandem efficiency.

An n^+/p shallow-homojunction design (~30nm deep) identical to that used for high-efficiency InP single-junction cells [ref. 4] is employed for the top cell, whereas the GaInAs bottom cell utilizes a p^+/n deep-junction design (0.25-0.50μm deep) which takes advantage of the natural minority carrier confinement provided by the InP layers on the back surface of the GaInAs base layer and the front surface of the GaInAs emitter. The InP top cell responds to photons with energies above 1.35eV, while the GaInAs bottom cell responds to photon energies in the 0.75-1.35eV range. Thus, the tandem exhibits an extremely wide response range which extends from the ultraviolet to well into the infrared (out to 1.65μm). The tandem offers the additional advantage of employing a radiation-resistant InP top cell which should result in higher end-of-life/beginning-of-life (EOL/BOL) efficiency ratios as compared to AlGaAs/GaAs or GaAs/Ge tandem cells, for example.

Tandem Performance Modeling

Computer modeling studies have been used to evaluate the performance potential of the tandem under different operating conditions. The results shown in table 1 were calculated assuming unity absolute extemal quantum efficiency (AEQE) when computing the short-circuit current density (J_{sc}). However, realistic parameters characterizing the junction behavior were employed, including an ideality factor (n) of 1.03, along with the following form for the reverse-saturation current density (J_0)

$$J_0 = \beta(E_g)T^3\exp(-E_g/kT) \quad [1]$$

where

$$\beta(E_g) = 3.85 * 10^{(0.24E_g)}\text{mA cm}^{-2}\text{K}^{-3} \quad [2]$$

In these expressions, E_g is the bandgap (in eV) at absolute temperature T and k is Boltzmann's constant. $\beta(E_g)$ was determined by fitting to open-circuit voltage/short-circuit current density (V_{oc}/J_{sc}) data for actual state-of-the-art cells measured at SERI covering a wide bandgap range (0.75-1.93eV) and employing the usual expression for J_0 as a function of V_{oc} and J_{sc} given by

$$J_0 = J_{sc}/\{\exp[qV_{oc}/nkT] - 1\} \quad [3]$$

Spectral and total irradiance values used for the AM0 spectrum were those recommended by the World Radiation Research Laboratory (1365.3 Wm^{-2}) [ref. 7]. Owing to the three-terminal tandem configuration, the top and bottom subcells were considered as being independently connected such that the computed tandem efficiency is equal to the sum of the individual subcell efficiencies in the stacked configuration. The bandgaps for InP and GaInAs at 25°C and 80°C were taken as 1.35 eV and 1.33 eV, and 0.75 eV and 0.73 eV, respectively. Additional details regarding the tandem cell model have been outlined in a previous paper [ref. 8]. The present modeling method represents a similar, but improved, procedure for calculating potential cell performance.

Although the bandgap combination offered by the InP/GaInAs tandem system is not the optimum for AM0 operation at 1 sun [ref. 8], the modeled efficiencies are quite respectable and represent 90-97% of the achievable maximum depending upon the operating temperature. The data in table 1 indicate that efficiencies of 26.9-33.0% are possible for operating temperatures in the 25-80°C range. As the concentration ratio is increased, the optimum-bandgap-pair values decrease due to the direct logarithmic dependence of V_{oc} and the fill factor (FF) on the ratio J_{sc}/J_0. As

a consequence, the InP/GaInAs bandgap combination is nearly optimum for concentration ratios in the 100-1000 range. The tandem efficiency increases substantially with increased concentration, particularly the contribution from the GaInAs bottom cell, and efficiencies of 34.7-42.7% are predicted for operation at 100-1000 suns. The concentration effect is especially pronounced and important for operation at higher temperatures. Note that the InP top cell is responsible for 73.5-83.6% of the total tandem efficiency under the range of conditions considered, thus emphasizing the need to develop high-performance InP cells in order to realize high tandem cell efficiencies. Nevertheless, the GaInAs bottom cell provides an impressive efficiency boost under all conditions due to the abundance of infrared radiation in the AM0 spectrum to which the InP cell is transparent. Using an arbitrary reduction factor of 0.75 to account for practical cell losses, it is concluded that practical AM0 efficiencies of 25-32% should be possible with the InP/GaInAs three-terminal tandem cell.

Performance of Component Subcells

Individual top and bottom cells have been fabricated and tested as a means of establishing a basis for assessing the highest achievable three-terminal tandem efficiency using current cell technologies. Figure 2 gives illuminated current/voltage (LIV) data under the AM0 spectrum, 25°C for a typical high-performance n/p InP shallow-homojunction (SHJ) cell without an ARC. The cell exhibits an efficiency of 12.4%, which would increase to ~17.5-18% with an optimally designed two-layer ARC. In a previous report [ref. 9], it was shown that the maximum efficiency of InP SHJ cells is limited by the relatively low values of the short-wavelength response and V_{oc}, both of which can be attributed to excessive surface recombination in the emitter layer. Effective passivation of the emitter surface will be necessary in order to realize InP cells with efficiencies approaching the theoretical limit. Moreover, the development of passivation techniques will allow deep-junction InP cells to be fabricated which will result in several advantages, including: i) a more robust cell design due to the deeper junction, ii) reduced performance sensitivity to junction depth variations and iii) reduced emitter sheet resistance, thus allowing the production of efficient InP concentrator cells, a key to achieving ultra-high efficiencies with the InP/GaInAs tandem cell.

LIV data for a p/n GaInAs cell with a 5μm-thick p-InP capping/window layer tested under similar conditions are shown in figure 3. The thick InP capping layer has been included on the GaInAs cell to simulate the optical filtering effected by an overlying InP top cell in the tandem configuration. An efficiency of 4.2% is observed for the low-bandgap GaInAs cell thus illustrating that the bottom cell offers a substantial efficiency gain over an InP cell alone, a result which is consistent with the modeling calculations for the InP/GaInAs tandem. It should be noted that large spectral mismatch corrections [ref. 10] (e.g., minus 20-30%) are typically necessary when measuring such low-bandgap devices using a Si reference cell to set the intensity

of a standard simulator (e.g., a Spectrolab X25) since most simulators are red-rich compared to the standard AM0 spectrum and, therefore, tend to give inflated J_{sc} values for cells with bandgaps below 1.0 eV. Another interesting characteristic of GaInAs cells with thick overlying InP filters is that their AM0 efficiency is actually higher than their global efficiency due to the absence of atmospheric absorption bands in the AM0 spectrum.

AEQE data for the same GaInAs cell, given in figure 4, show a high, "boxcar"-like response over the entire wavelength range (930-1650 nm) and sharp cutoffs at the bandgaps of both InP and GaInAs which indicate: i) complete optical filtering and effective surface passivation by the InP cap and ii) high-quality n-GaInAs base material and back surface minority carrier confinement by the n-InP buffer layer, respectively. From these results, it appears that the GaInAs junctions are at an advanced stage of development.

Using the results obtained for each of the component subcells, a combined tandem AM0 efficiency of 16.6% at 1 sun (25°C, no ARC) appears possible which would increase to 23-24% with an ARC. Additionally, the large increase in efficiency anticipated for operation at high solar concentration has been verified, at least partially, through flash-test concentrator LIV measurements performed at Sandia National Laboratories on SERI-grown GaInAs concentrator cells. For these cells, values of V_{oc} as high as 530mV have been observed at a concentration ratio of 471 suns. The above results demonstrate that the performance potential for the InP/GaInAs tandem cell is very high.

Epilayer Growth Procedures and Tandem Device Processing

The InP/$Ga_{0.47}In_{0.53}As$ heteroepitaxial device structures were grown by atmospheric-pressure metalorganic vapor phase epitaxy (APMOVPE) in a specially designed, homebuilt reactor system using trimethylindium, trimethylgallium, phosphine and arsine as the primary reactants with hydrogen sulfide and diethylzinc as the n- and p-type dopant sources, respectively. Growth was carried out on (100)-oriented, single-crystal InP substrates in a hydrogen ambient using a high-purity graphite susceptor inductively heated to 650°C. The structures were grown in a continuous manner without employing stopgrowth techniques at the heterointerfaces. Transmission electron microscopic (TEM) examination of InP/GaInAs multiple-quantum-well test structures grown in the same reactor has verified that extremely abrupt InP/GaInAs heterointerfaces (1-2 monolayers wide) are achieved using the current reactor design in the continuous growth mode. Additional characterization of the InP/GaInAs structures, using techniques such as photoluminescence (PL), electron probe microanalysis (EPMA), electron-beam-induced current (EBIC) and selective wet-chemical etching, has shown that the epitaxial growth process is under a level of control sufficient to produce high-performance tandem devices.

Prototype n/p/n InP/GaInAs tandems were successfully fabricated using the epitaxial device structure illustrated in figure 5. The structures were grown on n^+-InP substrates (S-doped) and consisted of the following sequence of layers: (i) an n-InP buffer layer, 0.5μm thick, which forms a minority carrier mirror for the back surface of the n-GaInAs base layer, (ii) an n-GaInAs base layer, 6μm thick, (iii) a p^+-GaInAs emitter layer, 200nm thick, (iv) a p^+-InP non-photoactive intermediate layer, 6μm thick, which serves to passivate the p^+-GaInAs emitter layer and also provides a conductive pathway for lateral current flow to the middle contact from both junctions, thus lowering the sheet resistance sufficiently to allow the use of a single middle contact gridline as explained in following sections, (v) a p^+-GaInAs stop-etch layer, 18nm thick, which facilitates correct placement of the middle contact, (vi) a p^+-InP back-surface field layer, 1μm thick, to enhance minority carrier confinement in the p-InP base layer, (vii) a p-InP base layer, 5μm thick and (viii) an n^+-InP emitter layer, 30nm thick.

Ohmic contacts to the back surface of the n^+-InP substrate (back contact) and the surface of the InP cell emitter layer (top contact) were formed by electroplating pure Au without annealing. The middle contact to the GaInAs stop-etch layer was formed by electroplating a three-layer metallization of Au/Zn/Au which was then annealed at 395°C for 1 minute in forming gas ($10\%H_2/N_2$). Wet chemical etching of the middle contact trough and the mesa isolation troughs was accomplished using the $10H_2SO_4$:$1H_2O_2$: $1H_2O$/Concentrated HCl system (both at room temperature) which etches the InP/GaInAs materials system selectively. $10H_2SO_4$:$1H_2O_2$:$1H_2O$ etches GaInAs at approximately 0.8 μm min^{-1}, whereas it attacks InP at an extremely slow rate (about 10 nm $min.^{-1}$). In contrast, concentrated HCl etches InP at about 8 μm $min.^{-1}$ and attacks GaInAs at only 25 nm $min.^{-1}$. The use of a thin GaInAs stop-etch layer in combination with the selective etching system makes correct placement of the middle contact in the structure a relatively straightforward procedure, and still allows for high transmission of sub-InP-bandgap photons to the GaInAs junction. The prototype tandem devices were tested without ARC's.

A long, narrow device geometry (1 cm x 0.165 cm overall dimensions) was used for the prototype devices in a "unit-cell" approach to testing the tandem concept as a precursor to developing three-terminal devices with fully interdigitated top/middle grids and square mesa geometries. This approach allowed for an array of five electrically isolated tandem cells from each growth run. The top/middle contact metallization scheme for the prototype consists of a middle contact pad at one end of the device with an associated single gridline, both of which are recessed (as described above) and interdigitated with a four-finger grid top contact facing the opposite direction with a contact pad at the other end. Details of the metallization and device mesas are shown in figure 6. The grid line parameters, including the width, height and spacing, were optimized for both the top and middle contacts using a computer model, with the sheet resistance, contact resistance and bulk metal resistivity as input parameters. The area required for the middle contact pad on the GaInAs stop-etch layer results

in a significant reduction of the top cell total area (0.140 cm^2 compared to 0.165 cm^2 for the bottom cell), thus, in practice, an aperture is used to illuminate selectively the intermediate region between the top and middle contact pads when performing LIV measurements.

Prototype Tandem Cell Performance

Completed tandem cells were characterized using AEQE and LIV techniques to assess current performance and also to identify areas for improvement. Composite AEQE data for one of the better tandems are shown in figure 7. Each component cell exhibits AEQE spectra which are essentially identical to those observed for high-performance top and bottom cells fabricated individually, which demonstrates that the integrity of the individual cells is maintained during the tandem growth and fabrication procedures. Note that the peak AEQE for the GaInAs cell (~81%) is substantially higher than for the InP cell (~66%) which is probably due to optical interference provided by the GaInAs stop-etch layer resulting in a mild antireflection effect for the GaInAs bottom cell.

Figure 8 shows composite LIV data for one of the better tandems measured under the global spectrum using an aperture to define the illuminated area (0.0822 cm^2), which corresponded to approximately one-half of the total junction area (0.165 cm^2). During these measurements, the cell not being tested was not connected to a load (i.e., it was left as an open circuit). The combined top cell/bottom cell efficiency is 15.4% global (roughly equivalent to 14% AM0) which would increase to ~22% global (~20 AM0) with a two-layer ARC.

Although the initial tandem efficiencies are encouraging, they fall short of the expected performance based on the results obtained with the individual top and bottom subcells. However, several possibilities for improving the tandem cell performance exist which should be relatively straightforward to implement. The present tandem device design suffers from several loss mechanisms which can be delineated as follows: i) the top/middle contact metallization results in excessive obscuration of the bottom cell, while the middle contact trough leads to a substantial loss of top cell area, ii) use of an aperture during LIV measurements results in a decreased value of J_{sc}/J_0 which lowers the V_{oc} and FF of both the top and bottom cells, iii) the InP top cell performance is limited by surface recombination and iv) optical reflection is high.

Solutions to the above-mentioned problems, in the order listed, include: i) application of Entech prismatic covers to reduce optical losses due to grid obscuration and to redirect light away from the middle contact troughs back into the InP top cell, ii) development of improved fully interdigitated grids with reduced bus-bar (contact pad) areas, thus eliminating the need to use apertures when performing LIV measurements, iii) development of emitter surface passivation techniques for InP cells.

Methods under current investigation include the use of lattice matched $Al_{0.48}In_{0.52}As$ pseudomorphic $Ga_xIn_{1-x}P$ window layers and iv) development of optimally designed ARC's. This task will require a detailed knowledge of the optical constants $n(\lambda)$ and $k(\lambda)$ of doped InP and GaInAs in order to model correctly the optical characteristics of the tandem stack. These data are currently unavailable, however, methods for determining such information are presently under development at SERI.

Conclusion

The InP/GaInAs three-terminal tandem cell is a promising photovoltaic device for achieving ultra-high efficiencies, high power-to-mass ratios and high EOL/BOL efficiency ratios in space power applications. Early experimental results regarding the fabrication and performance of this novel tandem cell have demonstrated its potential in these areas. Methods for improving the tandem cell efficiency have been identified and efforts to realize the full practical potential of the device are currently underway.

References

[1.] S. M. Vernon, S. P. Tobin, C. Bajgar, V. E. Haven, L. M. Geoffroy, D. R. Lillington and R. E. Hart, *Proc. NASA Conf. Space Photovoltaic Research and Technology*, 167, 1988.

[2.] N. P Kim, B. J. Stanbery, R. P. Gale and R. W. McClelland, *Proc. NASA Conf. Space Photovoltaic Research and Technology*, 138, 1988.

[3.] H. C. Hamaker, M. Grounner, N. R. Kaminar, M. S. Kuryla, M. J. Ladle, D. D. Liu, H. F. MacMillan, L. D. Partain, G. F. Virshup, J. G. Werthen and J. M. Gee, *Proc. NASA Conf. Space Photovoltaic Research and Technology*, 292, 1988.

[4.] M. W. Wanlass, T. A. Gessert, K. A. Emery and T. J. Coutts, *Proc. 20th IEEE PVSC*, 491, 1988.

[5.] L. Mayet, M. Gavand, B. Montegu and A. Laugier, *Proc. 20th IEEE PVSC*, 597, 1988.

[6.] L. M. Fraas, B. K. Shin, J. A. Cape, R. A. Ransom and D. E. Sawyer, *Proc. 16th IEEE PVSC*, 655, 1982.

[7.] C. Wehrli, *Physical Meteorological Observatory and World Radiation Center, tech. rep. 615*, Davos-Dorf, Switzerland, 1985.

[8.] M. W. Wanlass, K. A. Emery, T. A. Gessert, G. S. Horner, C. R. Osterwald and T. J. Coutts, *Proc. 9th PVAR&D Meeting*, 1989. To be published in Solar Cells.

[9.] M. W. Wanlass, G. S. Horner, T. A. Gessert and T. J. Coutts, *Proc. 1st Intemational Conference on Indium Phosphide and Related Materials for Advanced Electronic and Optical Devices*, 1989. To be published by SPIE.

[10.] C. R. Osterwald, Solar Cells **18**, 269, 1986.

Table 1. Computer modeling summary of the performance of an InP/$Ga_{0.47}In_{0.53}As$ independently connected tandem solar cell under AM0 illumination as a function of the operating temperature and solar concentration ratio.

Temperature (°C)	Concentration Ratio	InP Top Cell Efficiency (%)	$Ga_{0.47}In_{0.53}As$ Bottom Cell Efficiency(%)	Tandem Cell Efficiency (%)
25	1	25.9	7.1	33.0
	10	27.8	8.5	36.3
	100	29.6	9.9	39.5
	1000	31.4	11.3	42.7
80	1	22.5	4.5	26.9
	10	24.7	6.1	30.8
	100	26.9	7.8	34.7
	1000	29.1	9.4	38.5

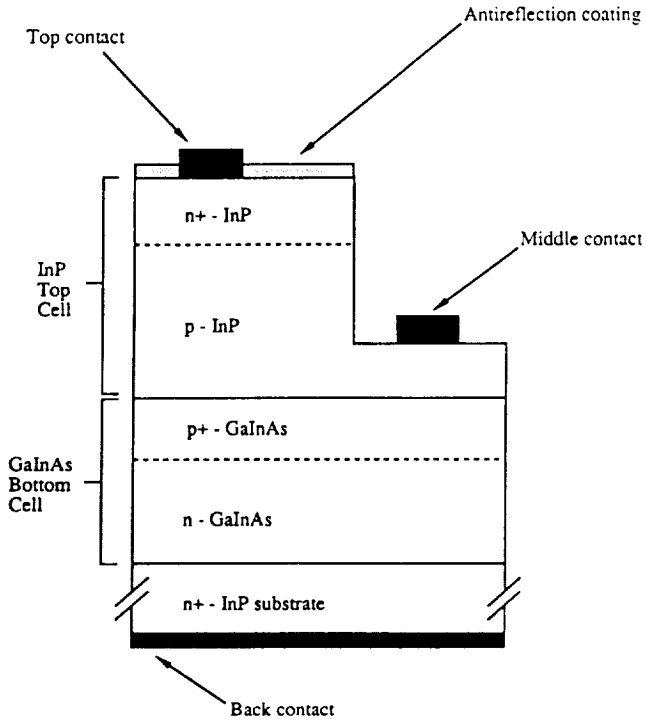

Figure 1. Schematic cross sectional diagram of the InP/$Ga_{0.47}In_{0.53}As$ three-terminal tandem solar cell.

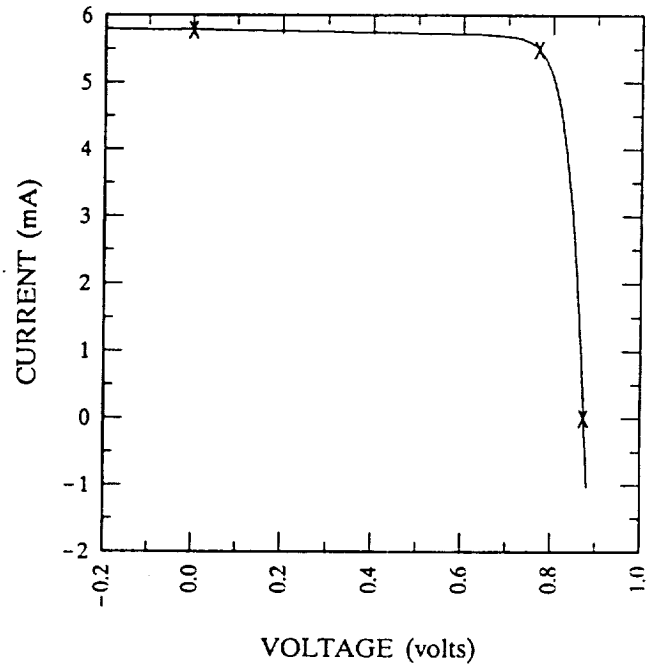

V_{oc} = 0.8735 volts
I_{sc} = 5.782 mA
J_{sc} = 23.13 mA/cm²
P_{max} = 4.224 mW
Fill factor = 83.64 %
I_{max} = 5.496 mA
Efficiency = 12.4 %
V_{max} = 0.7686 V

Figure 2. LIV data for a high-performance n/p InP shallow-homojunction solar cell (AM0, 25°C, no ARC).

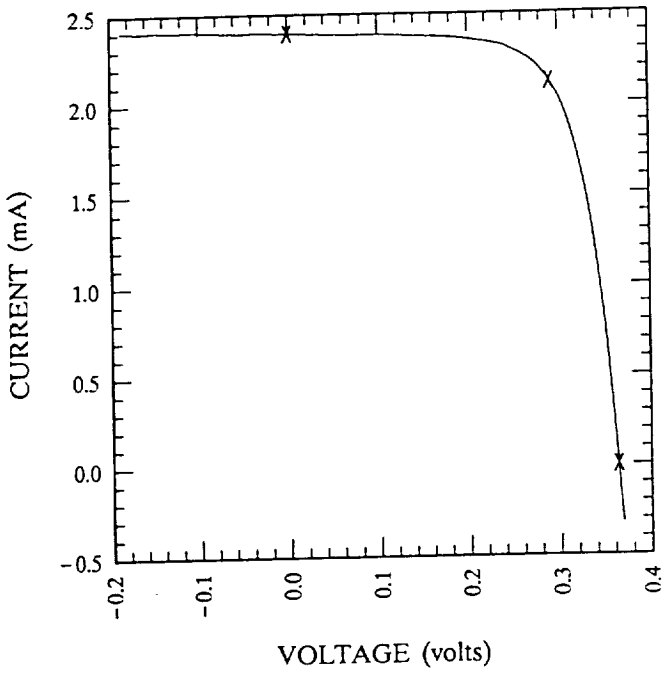

V_{oc} = 0.3635 volts
I_{sc} = 2.397 mA
J_{sc} = 22.19 mA/cm²
P_{max} = 0.615 mW
Fill factor = 70.62 %
I_{max} = 2.119 mA
Efficiency = 4.2 %
V_{max} = 0.2904 V

Figure 3. LIV data for a high-performance p/n $Ga_{0.47}In_{0.53}As$ solar cell with a 5μm-thick InP capping layer (AM0, 25°C, no ARC).

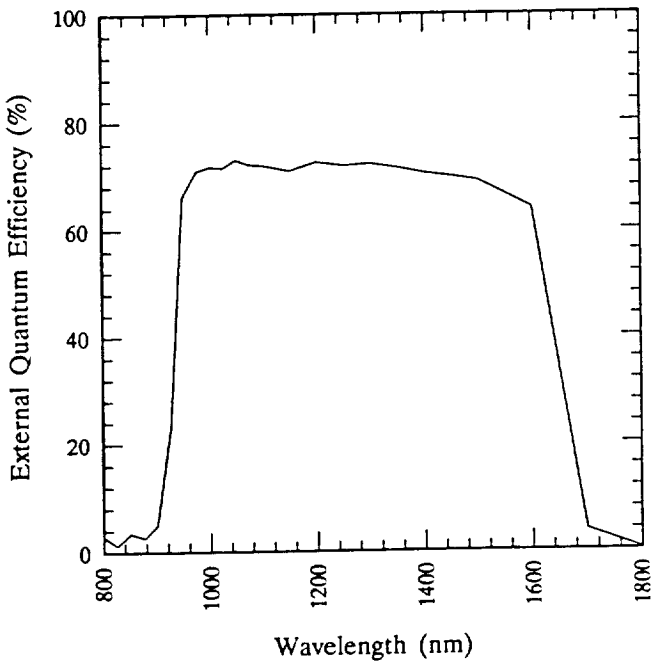

Figure 4. AEQE data (no ARC) for the $Ga_{0.47}In_{0.53}As$ cell with LIV data given in figure 3.

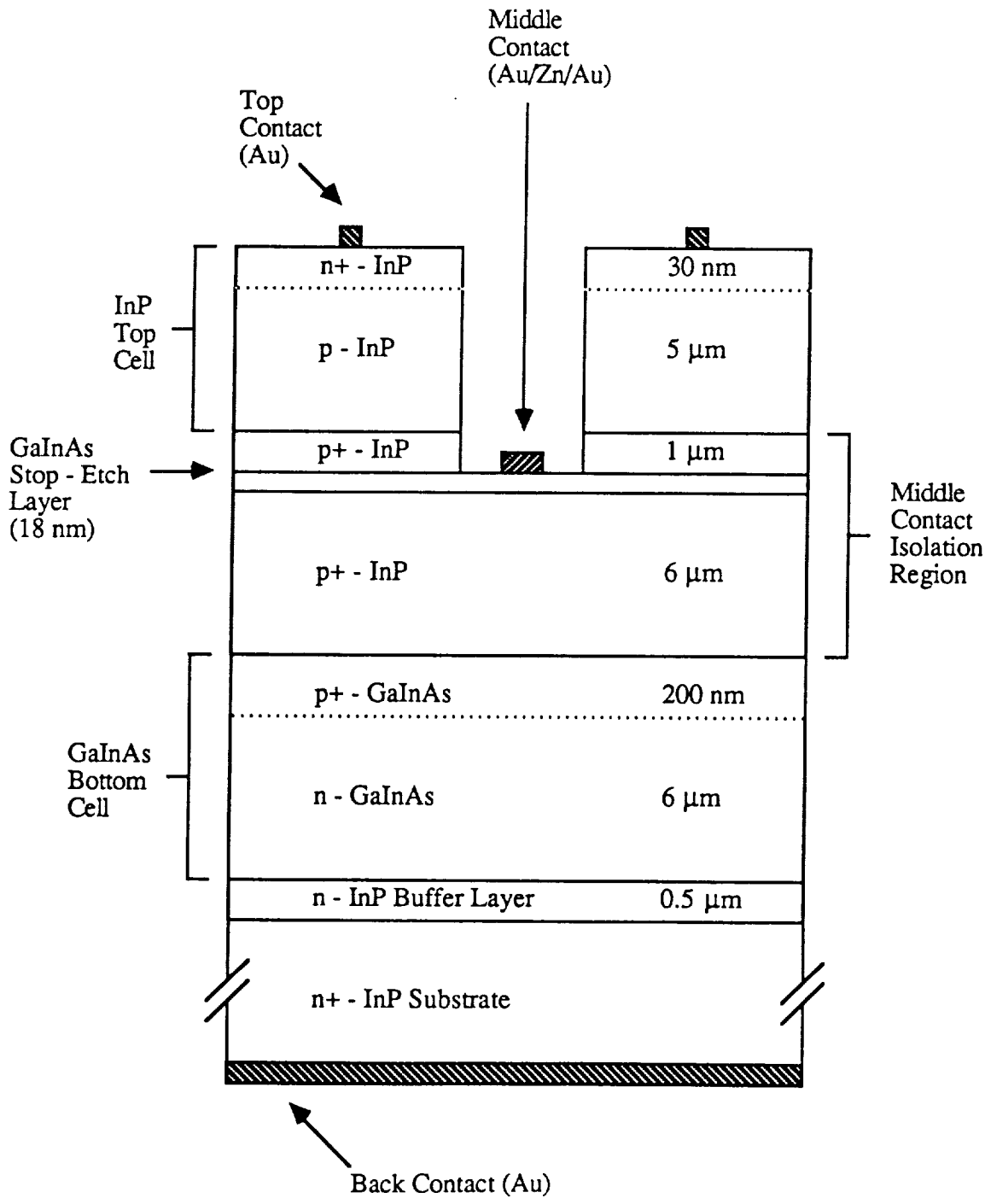

Figure 5. Cross sectional diagram of the prototype InP/$Ga_{0.47}In_{0.53}As$ three-terminal tandem solar cell structure.

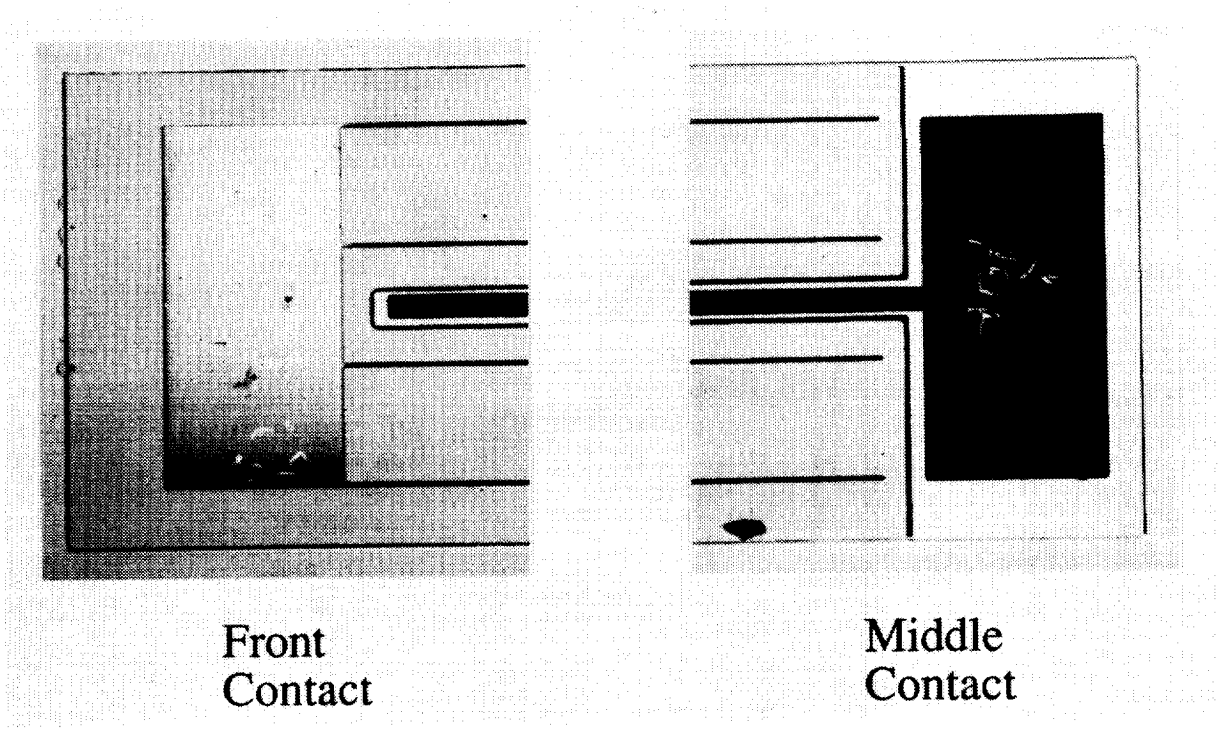

Figure 6. Optical micrographs showing details of the front and middle contact areas (plan view, 40X) on an actual prototype InP/$Ga_{0.47}In_{0.53}As$ three-terminal tandem cell.

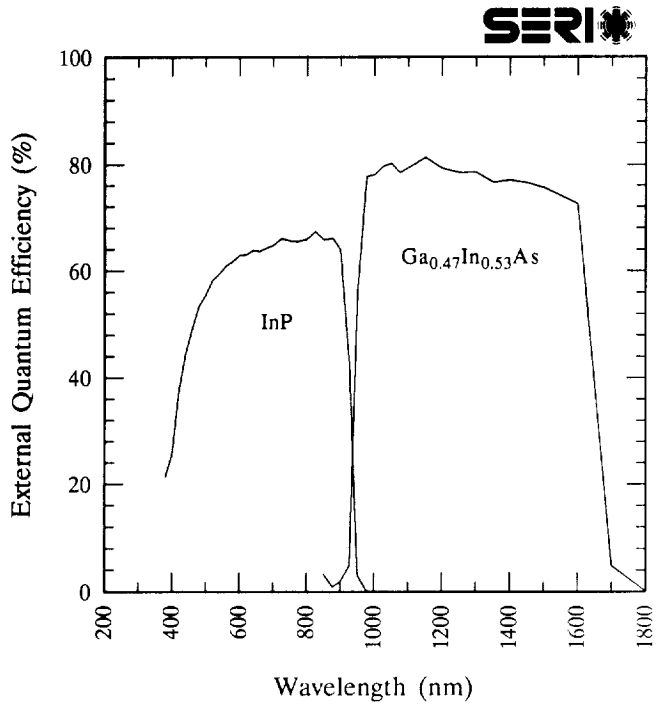

Figure 7. Composite AEQE data (no ARC) for an n/p/n InP/$Ga_{0.47}In_{0.53}As$ tandem cell.

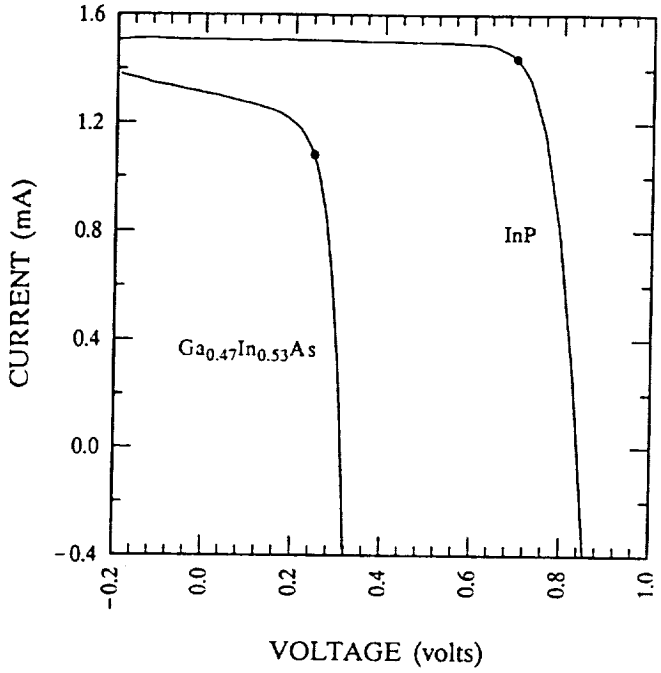

InP Top Cell	$Ga_{0.47}In_{0.53}As$ Bottom Cell
V_{oc} = 0.838 V	V_{oc} = 0.310 V
J_{sc} = 18.4 mAcm^{-2}	J_{sc} = 15.9 mAcm^{-2}
FF = 0.794	FF = 0.647
Eff. = 12.2 %	Eff. = 3.2 %

Figure 8. Composite LIV data (Global, 25°C, no ARC) for an InP/ $Ga_{0.47}In_{0.53}As$ three-terminal tandem cell using an aperture to define the illuminated area.

Session 2
GaAs Cells